Systems analyses of the Fabry kidney transcriptome and its response to enzyme replacement therapy identified and cross-validated enzyme replacement therapy-resistant targets amenable to drug repurposing

Check for updates

OPEN

Nicolas Delaleu[1,2,15], Hans-Peter Marti[2,3,15], Philipp Strauss[2], Miroslav Sekulic[4], Tarig Osman[2], Camilla Tøndel[2,5], Rannveig Skrunes[2,3], Sabine Leh[2,6], Einar Svarstad[2,3], Albina Nowak[7], Ariana Gaspert[8], Elena Rusu[9,10], Ivo Kwee[11], Andrea Rinaldi[12], Arnar Flatberg[13,14] and Oystein Eikrem[2,3]

[1]2cSysBioMed, Contra, Switzerland; [2]Department of Clinical Medicine, University of Bergen, Bergen, Norway; [3]Department of Medicine, Haukeland University Hospital, Bergen, Norway; [4]Department of Pathology and Cell Biology, Columbia University, New York, New York, USA; [5]Department of Pediatrics, Haukeland University Hospital, Bergen, Norway; [6]Department of Pathology, Haukeland University Hospital, Bergen, Norway; [7]Department of Endocrinology and Clinical Nutrition, University Hospital Zurich and University of Zurich, Zurich, Switzerland; [8]Department of Pathology and Molecular Pathology, University Hospital Zurich, Zurich, Switzerland; [9]Department of Nephrology, Fundeni Clinical Institute, Bucharest, Romania; [10]Department of Nephrology, Carol Davila University of Medicine and Pharmacy, Bucharest, Romania; [11]BigOmics Analytics, Lugano, Switzerland; [12]Institute of Oncology Research, Oncology Institute of Southern Switzerland, Università della Svizzera Italiana, Bellinzona, Switzerland; [13]Central Administration, St. Olav's Hospital, Trondheim University Hospital, Trondheim, Norway; and [14]Department of Clinical and Molecular Medicine, Faculty of Medicine and Health Sciences, Norwegian University of Science and Technology, Trondheim, Norway

Fabry disease is a rare disorder caused by variations in the alpha-galactosidase gene. To a degree, Fabry disease is manageable via enzyme replacement therapy (ERT). By understanding the molecular basis of Fabry nephropathy (FN) and ERT's long-term impact, here we aimed to provide a framework for selection of potential disease biomarkers and drug targets. We obtained biopsies from eight control individuals and two independent FN cohorts comprising 16 individuals taken prior to and after up to ten years of ERT, and performed RNAseq analysis. Combining pathway-centered analyses with network-science allowed computation of transcriptional landscapes from four nephron compartments and their integration with existing proteome and drug-target interactome data. Comparing these transcriptional landscapes revealed high inter-cohort heterogeneity. Kidney compartment transcriptional landscapes comprehensively reflected differences in FN cohort characteristics. With exception of a few aspects, in particular arteries, early ERT in patients with classical Fabry could lastingly revert FN gene expression patterns to closely match that of control individuals. Pathways nonetheless consistently altered in both FN cohorts pre-ERT were mostly in glomeruli and arteries and related to the same biological themes. While keratinization-related processes in glomeruli were sensitive to ERT, a majority of alterations, such as transporter activity and responses to stimuli, remained dysregulated or reemerged despite ERT. Inferring an ERT-resistant genetic module of expressed genes identified 69 drugs for potential repurposing matching the proteins encoded by 12 genes. Thus, we identified and cross-validated ERT-resistant gene product modules that, when leveraged with external data, allowed estimating their suitability as biomarkers to potentially track disease course or treatment efficacy and potential targets for adjunct pharmaceutical treatment.

Kidney International (2023) **104,** 803–819; https://doi.org/10.1016/j.kint.2023.06.029

KEYWORDS: biomarkers; enzyme replacement therapy; Fabry nephropathy; laser capture microdissection; systems biology; transcriptome

Fabry disease (FD) is an X-linked disorder caused by variants in the lysosomal enzyme, α-galactosidase A (*GLA*) gene.[1] Classic FD is characterized by complete absence or little activity of α-galactosidase A in hemizygous males, which results in early disease onset.[2] Retaining some α-galactosidase activity, nonclassic cases commonly show later onset and less severe disease course. Because of the random X-chromosomal inactivation, disease progression is variable in females, ranging from nonprogressive asymptomatic carriers to a classic FD phenotype.[3]

As a consequence of variable globotriaosylceramide (GL-3) accumulation and downstream effectors of cellular injury in various cell types, FD is characterized by interpatient heterogeneity. In general, the disease progresses slowly, and the natural course in patients with classic FD typically

Correspondence: *Oystein Eikrem, Section of Nephrology, Department of Medicine, Haukeland University Hospital and Department of Clinical Medicine, University of Bergen, 5021 Bergen, Norway. E-mail: oystein.eikrem@uib.no*

[15]ND and H-PM contributed equally.

Received 3 June 2022; revised 19 May 2023; accepted 22 June 2023; published online 5 July 2023

Lay Summary

Fabry disease (FD) is a rare genetic enzyme deficiency affecting several organs, including the kidneys. This study provides a framework for precision medicine evaluating changes in gene expression in kidney biopsies from patients with FD and controls over a maximum period of 10 years. We obtained RNA-sequencing data from laser capture microdissected archival kidney biopsies before initiation of enzyme replacement therapy (ERT) from 2 independent FD cohorts. Tissue compartments characterized include glomeruli, arteries, proximal tubuli, and distal tubuli. This enabled computation of cohort-specific and cross-validated transcriptional landscapes associated with Fabry nephropathy. Integrating analogous data collected after ERT subsequently enabled categorization of biological themes, pathways, and genes with respect to their sensitivity to ERT. With drug repurposing in mind, members of these therapy-resistant molecular modules were consequently interrogated for known drug-target interactions. Taken together, this represents a framework using kidney biopsies and advanced data science to systematically contextualize complex biological data with respect to potential biomarkers and drug targets for FD.

demonstrates chronic kidney disease that culminates in kidney failure before the age of 50 years.[4,5] Excessive lysosomal storage of GL-3 can be detected in the kidneys with histopathology already in young children before albuminuria and decline in glomerular filtration rate.[4,6]

The impact of FD on kidney function is a major contributor to its morbidity and mortality.[1,7] Consequently, substituting endogenous α-galactosidase A via enzyme replacement therapy (ERT) reduces GL-3 deposits and attenuates progression of Fabry neuropathy (FN) in a substantial number of patients.[8] Unfortunately, current regimens do not show sufficient benefits in all relevant patients,[8,9] highlighting the need of understanding the complexity of ERT's impact on a molecular level. With such insight, more effective therapeutic options may be developed.

In contrast to addressing high interpatient heterogeneity in conditions affecting thousands of subjects, the lower prevalence of FD[5,10] precludes many current patient stratification and personalized medicine approaches.[11–13] By taking advantage of recent advances in biotechnology and data science, concepts less demanding on patient numbers, such as precision and molecular medicine, are at the center of this study.[14] As any subgrouping would further exacerbate the challenges related to small patient numbers,[12,13] it is imperative to propose new targets that are relevant for a maximum of patients.

Furthermore, response patterns of such targets to ERT should be well established and closely related to potential new treatment strategies adjunctive to today's standard of care and may include drug repurposing.[8,15] The latter renders drug development significantly faster and more cost-effective in an environment facing declining drug development efficiency.[12]

Thus, this study aims to do the following: (i) use laser capture microdissection (LCM) and generate gene expression profiles from glomeruli, proximal tubuli, distal tubuli, and small arteries using RNA sequencing (RNAseq); (ii) combine standard RNA-seq workflows with network science methods to infer the molecular basis of FN and its modulation in response to ERT over time; and (iii) on this basis, identify cross-validated molecular modules that may be druggable or serve as biomarkers.

METHODS

Patient cohort from Bergen, Norway (NO)

Core kidney biopsies ($n = 24$) were collected from 8 pediatric and young adult patients with FD from 2003 to 2014. Fabry kidney biopsies were obtained from the same patients at baseline pre-ERT ($n = 8$), after 3 to 5 years ($n = 8$), and after 8 to 10 years ($n = 8$) of ERT using a 16-gauge core biopsy needle. ERT consisted of agalsidase-β, 0.2 to 1 mg/kg body weight ($n = 3$; as described previously[16]) or agalsidase-α, 0.2 mg/kg body weight ($n = 5$). The varying dosages of agalsidase-β for a limited period were related to the shortages of agalsidase-β, leading to involuntary dose reductions[17] (Table 1).

In addition, we have included control biopsies ($n = 8$) with normal-looking tissue from adolescents and adult patients of the Norwegian Kidney Biopsy Registry. These individuals represent some of the healthiest subjects within the Norwegian Kidney Biopsy Registry, and all presented normal histopathology. The biopsy indications among these patients included microscopic hematuria and slight elevations in creatinine and microalbuminuria.

Validation cohort from Switzerland and Romania (CHRO)

Kidney biopsies were obtained from adult patients with FN from Zurich, Switzerland ($n = 3$), and adult subjects from Bucharest, Romania ($n = 5$).

Kidney biopsies were obtained with a 16-gauge core biopsy needle from untreated patients ($n = 3$ biopsies) and ERT-treated patients ($n = 6$ biopsies) with a mean of 1.8 years on ERT; 1 patient contributed with a baseline biopsy and a follow-up biopsy while receiving ERT. Thereby, ERT consisted of agalsidase-β, 1 mg/kg body weight ($n = 4$), or agalsidase-α, 0.2 mg/kg body weight ($n = 2$; Table 1).

We have combined these patients ($n = 8$) with their kidney biopsies ($n = 9$) into a single validation cohort (CHRO) categorized as "baseline" ($n = 3$ biopsies; untreated or ERT <6 months) and >1 year on ERT ($n = 6$ biopsies). All patient characteristics are also provided in Table 1.

Kidney biopsy microdissection and RNA extraction

For identification of structures and annotations, 3-μm-thick sections from formalin-fixed, paraffin-embedded (FFPE) kidney biopsies stained with periodic acid–Schiff were used. Slides were scanned with Scanscope XT Aperio (Leica. Biosystems) at original magnification ×40, resulting in a resolution of 0.25 μm per pixel. Digitalized sections were viewed and annotated in Imagescope 12 (Leica Biosystems). Using a Zeiss PALM LCM system (Carl Zeiss AG), glomeruli, proximal tubuli, distal tubuli, and arteries were then microdissected from 10-μm-thick FFPE sections. Total RNA from all microdissected samples from the NO cohort ($n = 128$) and CHRO cohort ($n = 36$) was extracted using the High Pure FFPE RNA Isolation Kit (Roche Molecular Systems, Inc.).

Table 1 | Characteristics at baseline, 3 to 5 years, and 8 to 10 years for the NO cohort, characteristics at baseline and <6 and >12 months of ERT for the CHRO cohort, and characteristics for normal controls

	NO cohort			CHRO cohort			
Characteristic	Baseline, before ERT	ERT >3 to 5 yr	ERT >8 to 10 yr	Baseline or ERT <6 mo	ERT >12 mo	Normal controls	*P* value
No. of patients	8	8	8	8	8	8	
Sex	M:7, F:1			M:3, F:5		M:4, F:4	
Mutations	3 Missense, 5 truncating			6 Missense, 2 truncating			
Age at biopsy, yr	14 (7–30)	18 (12–35)	25 (17–39)	30 (17–50)	34.5 (21–57)	27 (11–37)	0.06
Age at ERT initiation, yr	14.5 (7–30)			30 (17–55)		NA	0.01
mGFR, ml/min per 1.73 m^2	106 (86–120)	97 (82–122)	91 (74–125)	NA	NA	NA	
eGFR, ml/min per 1.73 m^2	116 (95–126)	NA	NA	92 (55–134)	98 (47–119)	114 (76–147)	
Albumin-to-creatinine ratio, mg/mmol	5.4 (0.6–13.6)	10.1 (0.6–14)	4.4 (0.3–26.4)	11.3 (1.7–15.9)	8.3 (1.6–33.9)	22.5 (2.1–54)	0.35
Plasma GL-3, μmol/L	8.5 (2.7–10.2)	3.8 (3.5–5)	3.6 (2.3–4.4)	NA	NA	NA	
Plasma Lyso-GL-3, ng/ml	35.6 (11.9–130.7)	13.5 (4.7–25.6)	23.1 (2.2–39.5)	NA	NA	NA	
Podocyte composite score	7 (6.9–7)	4 (0.5–4.9)	5.58 (0.6–7)	NA	NA	NA	
ACE/ARB, *n*	0	1	2	1	3	0	

ACE, angiotensin-converting enzyme; ARB, angiotensin receptor blocker; CHRO, validation cohort from Switzerland and Romania; eGFR, estimated glomerular filtration rate; ERT, enzyme replacement therapy; F, female; GL-3, globotriaosylceramide; Lyso-GL-3, globotriaosylsphingosine; M, male; mGFR, measured glomerular filtration rate; NA, data not available; NO, patient cohort from Bergen, Norway.
Values are medians (ranges) unless otherwise indicated. Albumin-to-creatinine ratio reference, <2.5 mg/mmol creatinine; eGFR reference, >60 ml/min per 1.73 m^2; mGFR reference, >90 ml/min per 1.73 m^2 (glomerular filtration rate was measured by iohexol clearance); plasma GL-3 reference, 1.6 to 3.3 μmol/L; plasma Lyso-GL-3 reference, <2.0 ng/ml; podocyte composite score reference, 0 to 7. Podocyte composite score includes podocyte GL-3 inclusions and podocyte vacuolization. The ACE/ARB row displays the number of patients who were treated with this medicine around the time of the biopsy. All cohorts compared with either the Mann-Whitney *U* test or the Kruskal-Wallis test.

Quality and quantity of extracted RNA and sample numbers

Quality and quantity of the extracted RNA was determined as described below. In the NO samples, mean DV200 (percentages of fragments >200 nucleotides) values (95% confidence interval) were 58.8% (52.5%–65.0%). Mean concentration (95% confidence interval) of RNA was 1.07 (0.89–1.24) ng/sample. Taken together, we have obtained low, but sufficient, amounts of good quality RNA to generate gene expression profiles from 120 of 128 samples representing NO patients ($n = 8$).

From the Swiss-Romanian CHRO patient cohort ($n = 8$), we were also able to extract low amounts of good quality RNA with a mean (95% confidence interval) of 0.95 (0.66–1.23) ng/sample and a DV200 mean (95% confidence interval) of 67.2% (60.7%–73.6%). This allowed generating expression profiles from 38 of 44 nephron compartments. Twelve samples originated from 3 biopsies from untreated patients at baseline and, together with the remaining 6 biopsies ($n = 24$ samples) from ERT-treated subjects (mean, 1.8 years on ERT), thus defined the CHRO cohort.

RNA library preparation and sequencing

Total RNA concentration was quantified using a Qubit RNA HS Assay Kit on a Qubit 2.0 Fluorometer (Thermo Fisher Scientific Inc.). Integrity was measured using the Agilent RNA 6000 Pico Kit on a 2100 Bioanalyzer (Agilent Technologies), and the DV200 values were calculated. We used DV200, considered a reliable predictor of RNA quality in FFPE tissue,[18] before library preparation.

Subsequently, RNA-sequencing libraries were prepared using the standard Illumina Access protocol (RNA exome; Illumina) on an Illumina platform in different batches because of the large number of samples and at the following genomic facilities: (i) the Norwegian University of Science and Technology in Trondheim, Norway, in collaboration with Vidar Beisvåg and his group (NO patient cohort); (ii) Firalis SA, Huningue, France, in collaboration with Eric Schordan (NO cohort); and (iii) the Functional Genomics Center Zurich (CHRO), University of Zurich, Switzerland (NO and CHRO cohort).

Library normalization of the complete cohort was then performed at Norwegian University of Science and Technology. Libraries were normalized to 2.2 pM for the NextSeq 500 instrument, 2.2 pM for the HiSeq 2500, and 2.3 pM for the HiSeq 4000 instrument. Samples were then subjected to paired-end 2 × 75 base pair sequencing with ≈60 million paired-end reads per sample. Half of the glomerular compartment (NO cohort) was sequenced using an Illumina NextSeq 500 instrument, and the other half was sequenced on an Illumina HiSeq 2500 instrument. All other compartments from the NO cohort were split 5 to 3 between an Illumina HiSeq 4000 instrument and an Illumina HiSeq 2500 instrument. Normal controls were sequenced on an Illumina HiSeq 2500 instrument. The Swiss part of the CHRO cohort was sequenced on an Illumina HiSeq 4000 instrument. The Romanian part of the CHRO cohort was sequenced on a HiSeq 2500 instrument. Base calling was done on the HiSeq instrument by Illumina's Real Time Analysis 1.17.21.3. FASTQ files were generated using bcl2fastq v2.20 (Illumina, Inc.). Data will be made available in the repository Gene Expression Omnibus at https://www.ncbi.nlm.nih.gov/geo/ with accession number GSE 178947.

Statistical analysis and RNA data processing

Transcript expression values were generated by quasi alignment using Salmon (http://salmon.readthedocs.io/en/latest/index.html) and the Ensembl (GRCh38) human transcriptome. Aggregation of transcript to gene expression was performed using tximport (http://bioconductor.org/packages/release/bioc/html/tximport.html). An empirical expression filter was applied, which positively selected genes with >1 count per million in >25% of samples per data set.

Comparing patient characteristics

Differences between clinical characteristics of the different cohorts were assessed with the Mann-Whitney U test when comparing 2 patient groups, or the Kruskal-Wallis test when comparing >2 groups with each other. For all cases, significance threshold was set at $P \leq 0.05$.

Ethical approvals

All patients provided written informed consent or parental consent for children. The study was performed in accordance with principles of the Declaration of Helsinki and was approved by the Ethics Review Boards of the Western Norway Regional Health Authority (REK vest 2013/553), Zurich (Kantonale Ethikkommission Zürich, Gesuch BASEC-Nr. 2017-00662), and Bucharest (Fundeni Clinical Institute Board of Ethics, number 749, 2018).

Differential gene expression and pathway analyses

A Supplementary Glossary covers the concepts introduced below.

On the basis of unsupervised clustering and principal component analyses correlation, potential batch effects within the RNAseq data were mitigated using ComBat in combination with count per million normalization.[19] Subsequently, using a standard DESeq2 workflow, differential gene expression was assessed to compare all groups from the same compartment.[20] Ranked on the basis of $\log_2$ fold change, these lists, comprising 17,561 features (i.e., genes passing all criteria set by the analyses described above), were subsequently subjected to Fast Gene Set Enrichment Analysis[21] to assess concordant changes (1E + 06 permutations) within a total of 26,251 gene sets (GSs). Of the latter, 10,287 GSs passed the size thresholds set at ≥10 and ≤500 member genes, therewith mitigating the limitations of gene set enrichment analyses with respect to small or large GSs.

Mapping transcriptional landscapes

To avoid introducing arbitrary significance thresholds before the contextualization of changes in gene expression as a whole, a GS-based approach to analyzing these data was chosen.[22] A total of 26,251 GSs compiled, curated, and updated by research consortia, such as the Gene Ontology project and Reactome, were interrogated. The method for assembling this GS collection was previously described.[23] For this study, the resources were compiled on March 1, 2019.

To comprehensively assess Fast Gene Set Enrichment Analysis results for each compartment, they were mapped using network-based algorithms we described previously.[24–27] Taking advantage of having generated data from 2 independent patient groups, the NO and the CHRO cohorts, comparative transcriptional landscapes were computed to increase scope, whereas cross-validated transcriptional landscapes were extracted to focus on robustness. For the latter only, GSs yielding significant enrichment or depletion signal (adjusted $P <$ 0.05) for both cohorts when compared with normal controls (N_CTRL) were mapped.

All networks were organized by pair-wise forces of attraction (i.e., edge weights) exerted in cases where GSs share ≥10% of their member genes. With that, these networks *or* maps take into account pleiotropy of genes and functional redundancies inherent to complex biological systems.[25–28] To prevent isolated network areas, the largest overlap of <10% per GS, identified using the maximum spanning tree algorithm, was retained for GSs that did not meet a connectivity threshold of 10%.

For comparative transcriptional landscapes, simulating stochastic flow within the networks using the Markov cluster algorithm identified clusters within these networks. On the basis of the GSs' names, Fast Gene Set Enrichment Analysis–related statistics, as well as distribution and function of the specific genes underlying their significant enrichment or depletion signal (i.e., leading edge genes), the resulting clusters were then interpreted in detail. Subsequently, each cluster could be summarized and annotated with a term denoting the biological theme that the changes as a whole were associated with to infer. In cases aiding interpretation and communication of results, thematically related Markov cluster algorithm clusters were then combined into a common biological theme.

All transcriptional landscapes were drawn using the yFiles organic layout algorithm in Cytoscape 3.7.2[29] before interpretation and annotation. To allow direct comparison, results characterizing responses to ERT were mapped within these original network structures.

Estimating lysosome localization of the ERT-resistant genetic module

Integrating subcellular localization of gene protein products can improve the understanding of molecular data in a more specific context. As FD is a lysosomal storage disease, estimating lysosomal localization probabilities for protein products of the cross-validated ERT-resistance genetic module identified is meaningful. An integrated score, combining text mining, results from high-throughput screens, and predictions modalities[30] (as of November 14, 2019) of >2, was deemed adequate to assume a reasonable possibility for lysosomal localization.

Building the target::target::drug interactome

Target::target interactions among the 94 targets comprising the ERT-resistant molecular module for glomeruli and arteries were extracted from String V11.[31] All active interaction sources were considered, and a combined interaction score of ≥0.4, which equates to medium confidence, was required to validate a target::target interaction.

Target::drug interactions reflect data summarized in DrugBank 5.1.5's UniProt links source. The type of pharmacologic action per target::drug interaction was obtained via DrugBank's web interface based on the same version comprising 13,511 drug entries (March 1, 2010[32]). Considering the nature of the ERT-resistant molecular modules, the categories of activators (activator), agonists (agonist and partial agonist), inducers (inducer), ligands (ligand), and positive modulators (positive allosteric modulator, positive modulator, and agonist-positive allosteric modulator) were retained. Merging data form the different sources and final visualizations were completed using the yFiles organic layout algorithm in Cytoscape 3.7.2 as a basis.[29]

Immunohistochemistry of transferrin receptor

One of the interesting findings made based on mRNA was validated on the protein level with immunohistochemistry using 4-μm-thick FFPE kidney biopsy sections. The following primary antibody was used: Transferrin Receptor Monoclonal Antibody H68.4 (1:1000; monoclonal; mouse; catalog number 13-6800; Thermo Fisher Scientific). For negative controls, the primary antibody was omitted. Incubations were 1 hour at room temperature. Immunoreactivity was visualized using the EnVision system with 3,3′-diaminobenzidine (Agilent). Antigen retrieval was achieved at pH 6.0, and sections were counterstained with haematoxylin (number CS70030-2; Dako).

RESULTS

Comparative assessment of transcriptional landscapes pre-ERT

Having included 2 independent cohorts representative for FN (Table 1), this allowed for systematic estimation of inter-cohort variability with N_CTRLs as a common reference. This addresses issues of small cohorts with possibly skewed distributions for key aspects, such as age at diagnosis or

degree of organ dysfunction. Thus, to approximate the relevance of these factors, we systematically integrated all significant alterations in gene-expression patterns (i.e., GS per cohort into 1 comparative transcriptional landscape per compartment).

With an aggregate of 191 GSs passing significance thresholds for the NO cohort versus N_CTRLs or CHRO cohort versus N_CTRLs, glomeruli clearly displayed the highest degree of FD-specific alterations of all compartments (Figure 1; Supplementary Figure S1), followed by arteries with 72 GSs (Figure 2; Supplementary Figure S2). For the same 10,287 GSs assessed, tubular compartments exhibited 9 significant changes for proximal tubuli (Supplementary Figure S3) and 39 for distal tubuli (Supplementary Figure S4).

Cohort-specific differences in glomeruli's transcriptional landscape pre-ERT

Of the 191 GSs previously mentioned, 146 were mapped as a consequence of their significant dysregulation unique to the NO cohort. Similarly, 23 GS were mapped exclusively as a consequence of the CHRO versus N_CTRLs comparison (Figure 1; Supplementary Figure S1). That leaves 22 pathways coherently enriched or depleted in glomeruli of both cohorts. Although this limited overlap may, to a degree, be attributed to sample size, it may also be related to differences in cohort characteristics (Table 1).

Most important, no GS, for glomeruli or any other compartment, yielded diametrically opposed significant results. In other words, no GS was significantly enriched in one cohort versus N_CTRLs while being significantly depleted in the other or vice versa (Figures 1 and 2; Supplementary Figures S1–S4).

Despite the absence of this type of conflicting result, the fact that 88% of GSs mapped for glomeruli yielded significance in just one of the cohorts raises the question of how these cohorts are interrelated on a molecular basis. Assessing significance patterns per biological theme revealed that some were mapped entirely because of one cohort. That was true for the *Plasma membrane*, *Regulation of blood pressure*, *Cell division*, and *Mitochondria* themes (Figure 1; Supplementary Figure S1). Unsurprisingly, with exception of *Extracellular matrix and Epithelial-mesenchymal transition* and *Cell motility*, glomeruli from the NO cohort dominated all themes (Figure 1; Supplementary Figure S1). Interestingly, although themes such as *Innate immunity* showed a clear dichotomy regarding which processes were altered in what cohort, other themes, *Keratinization* in particular, comprised most GSs intersecting the 2 cohorts (Figure 1; Supplementary Figure S1). Cross-validation in such a manner point towards a universal validity and warrants additional analyses described below.

Cohort-specific differences in proximal and distal tubular transcriptional landscape pre-ERT

The biological state of both tubular compartments from the CHRO cohort was indistinguishable from N_CTRLs when defined via gene set enrichment analysis. Significant differences for these compartments could only be identified when comparing NO patients with N_CTRLs. For proximal tubuli, these alterations involved just 9 GSs pertaining to *Translation* (Supplementary Figure S3). Distal tubuli, on the other hand, primarily displayed gene-expression patterns specific for an immune component involving *Inflammation and chemotaxis*. Potentially related to the presence of such cells, other themes summarized enrichment of processes pertaining to cell motility and cell cycle regulation. In glomeruli and arteries alike, keratinization-specific GSs reemerged in distal tubuli of NO patients (Supplementary Figure S4).

Cohort-specific differences in arteries' transcriptional landscape pre-ERT

With 33 GSs of 72 (46%), consistently altered in both cohorts, changes in this compartment were the most coherent (Figure 2; Supplementary Figure S2). In contrast with glomeruli, and with exception of *Keratinization and intermediate filament*, average significance for all themes in arteries was more pronounced in CHRO versus N_CTRLs compared with NO versus N_CTRLs (Figure 2). Interestingly, enrichment in pathways of the *Complement system* was exclusive to the CHRO cohort (Figure 2; Supplementary Figure S2). This contrasts the observation of immune activation in distal tubuli exclusively observed for the NO cohort (Supplementary Figure S4). In both cases, the same pathways responsible for detection of stimuli seemed activated upstream, inducing somewhat different responses.

Degree of normalization within transcriptional landscapes in the presence of ERT over time

Mapping corresponding results from biopsies collected during follow-up onto the network structures presented in Supplementary Figures S1 to S4 revealed that ERT, to a large extent, induced reversal of FN-associated coordinated transcriptional alterations to levels comparable with N_CTRLs over time (Figure 3; Supplementary Figures S5–S8). This phenomenon was particularly evident in the NO cohort (Figure 3a–d; Supplementary Figures S5–S8A–C) and prominent for GSs uniquely dysregulated in this cohort (Figure 3c and d). The fact that no GSs for any compartment yielded significance when comparing molecular states between 10 and 5 years of ERT (Figure 3a–d; Supplementary Figures S5–S8D) further indicates stable molecular states after several years of ERT.

However, despite this quantitatively highly relevant effect of ERT, especially for arteries and to a lesser extent for glomeruli, some GSs reemerged or failed to normalize to levels comparable with N_CTRLs over time. Noticeably, the latter were greatly overrepresented in the group of GSs consistently yielding significance in both cohorts pre-ERT already and are therefore analyzed in detail below.

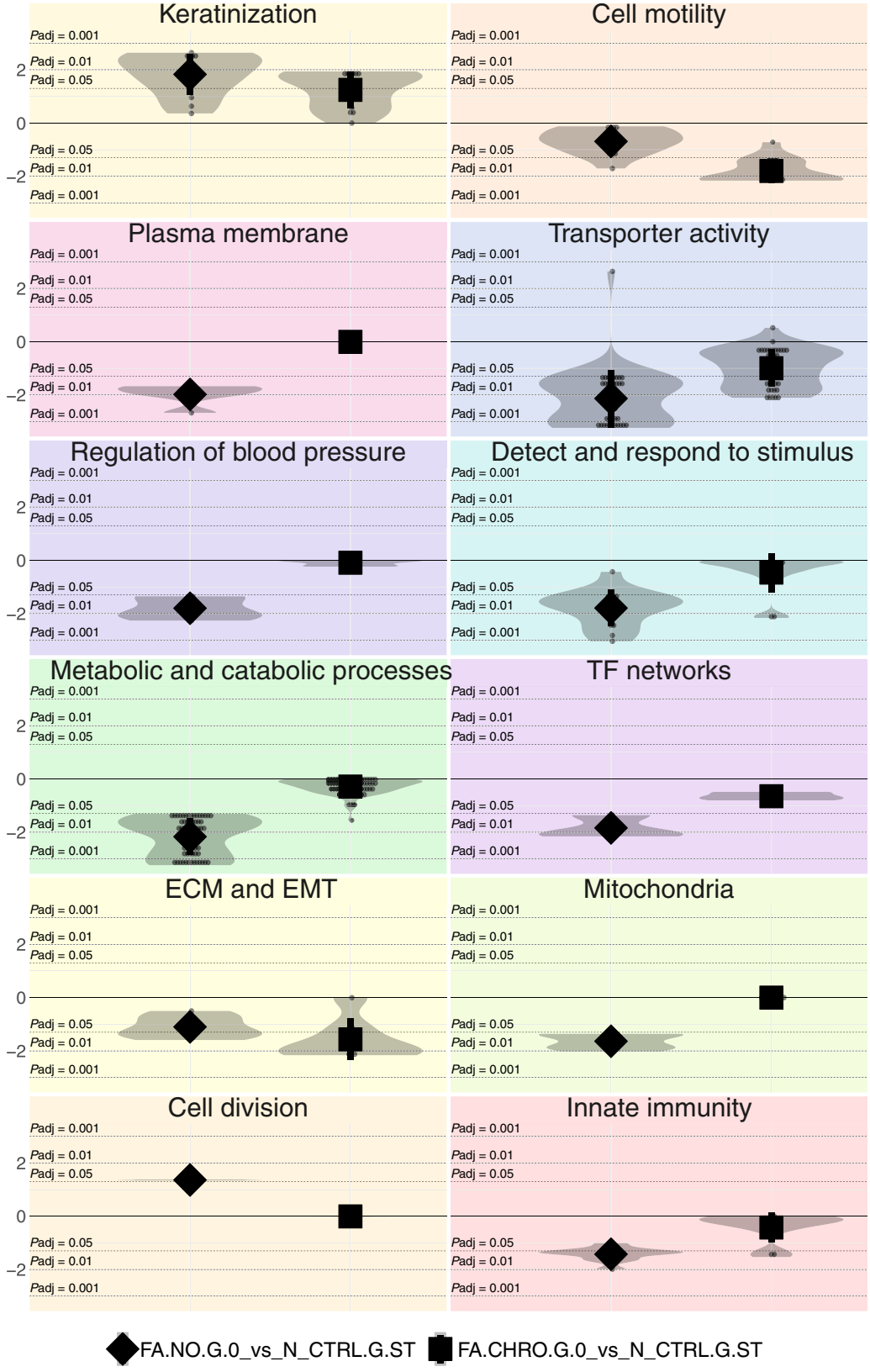

Figure 1 | Violin plots delineating the transcriptional landscape of glomeruli (Supplementary Figure S1) integrating similarities and differences between the patient cohort from Bergen, Norway (NO), and validation cohort from Switzerland and Romania (CHRO) before enzyme replacement therapy (ERT) versus N_CTRLs. Violin plots display directional adjusted *P* (*P*adj) values of the gene sets per biological theme for the comparisons indicated. Adjusted *P* values were log transformed ($\log_{10}$), and the algebraic sign was (continued)

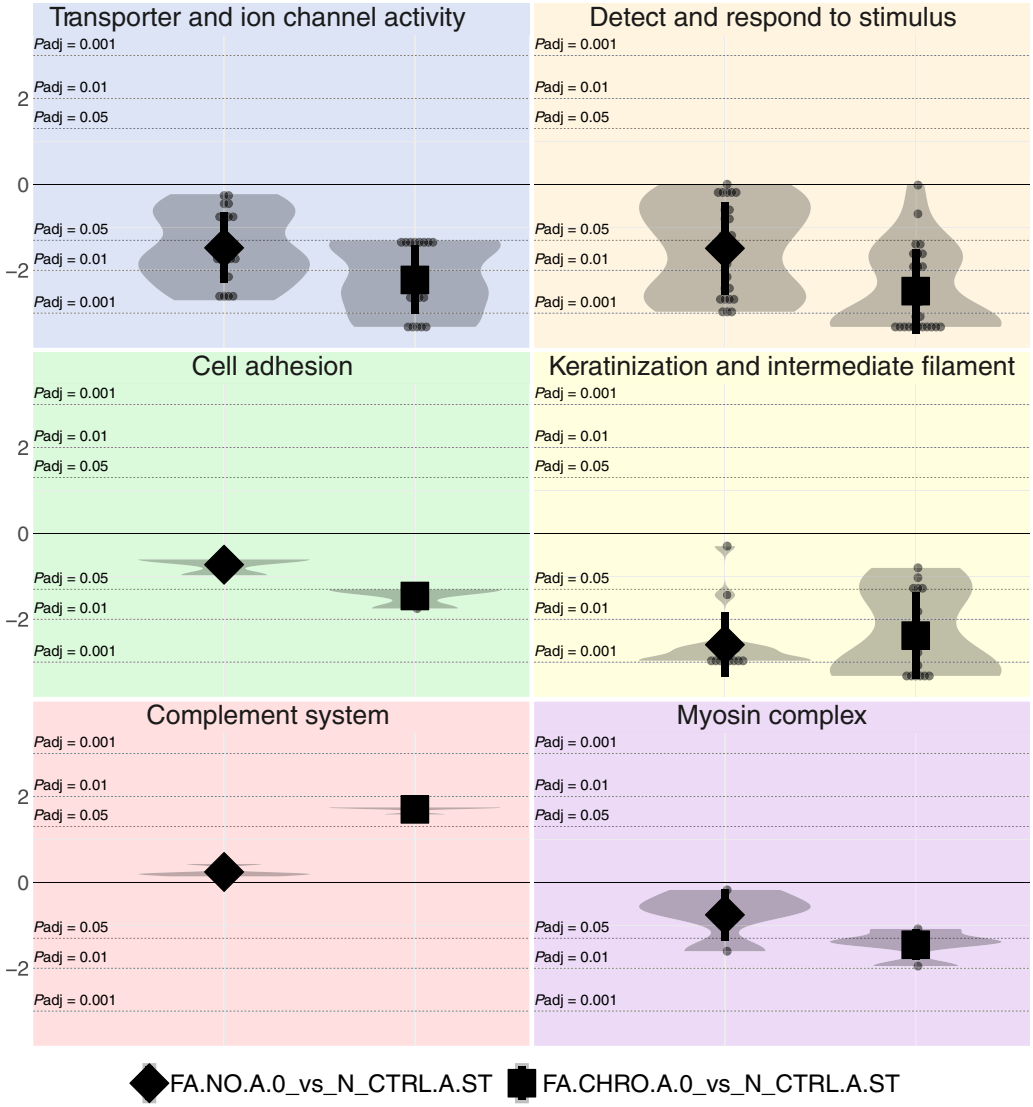

Figure 2 | Violin plots delineating the transcriptional landscape of arteries (Supplementary Figure S2) integrating similarities and differences between the patient cohort from Bergen, Norway (NO), and validation cohort from Switzerland and Romania (CHRO) before enzyme replacement therapy (ERT) versus N_CTRLs. Violin plots display directional adjusted *P* (*P*adj) values of the gene sets per biological theme for the comparisons indicated. Adjusted *P* values were log transformed (log_{10}), and the algebraic sign was assigned according to enrichment (positive) or depletion (negative). The solid horizontal line corresponds to an adjusted *P* of 1, whereas the dashed horizontal lines indicate significance levels of 0.05, 0.01, and 0.001 for enrichment and depletion, respectively. Bars indicate mean ± SD. FA.CHRO.A.0_vs_N_CTRL.A.ST, arteries pre-ERT or ERT < 6 months from patients with Fabry disease (FD) belonging to the CHRO cohort versus normal controls; FA.NO.A.0_vs_N_CTRL.A.ST, arteries pre-ERT from patients with FD belonging to the NO cohort versus normal controls.

Cross-validated transcriptional landscapes per compartment pre-ERT

The consistent finding of similar coordinated changes in gene expression pre-ERT in 2 independent cohorts represents a type of cross-validation. This raises confidence that mechanisms governed by these changes in gene expression could be valid for most patients with FD. Although such pathways were absent in proximal and distal tubuli, glomeruli and arteries yielded 22 (Figure 4a and b) and 33 GSs (Figure 5a and b), respectively, that passed all significance thresholds for both cohorts.

The fact that many of these GSs also resisted modulation after ERT, 77% for glomeruli (Figure 4e) and 91% for arteries

Figure 1 | (continued) assigned according to enrichment (positive) or depletion (negative). The solid horizontal line corresponds to an adjusted *P* of 1, whereas the dashed horizontal lines indicate significance levels of 0.05, 0.01, and 0.001 for enrichment and depletion, respectively. Bars indicate mean ± SD. ECM, extracellular matrix; EMT, epithelial-mesenchymal transition; FA.CHRO.G.0_vs_N_CTRL.G.ST, glomeruli pre-ERT or ERT < 6 months from patients with Fabry disease (FD) belonging to the CHRO cohort versus normal controls; FA.NO.G.0_vs_N_CTRL.G.ST, glomeruli pre-ERT from patients with FD belonging to the NO cohort versus normal controls.

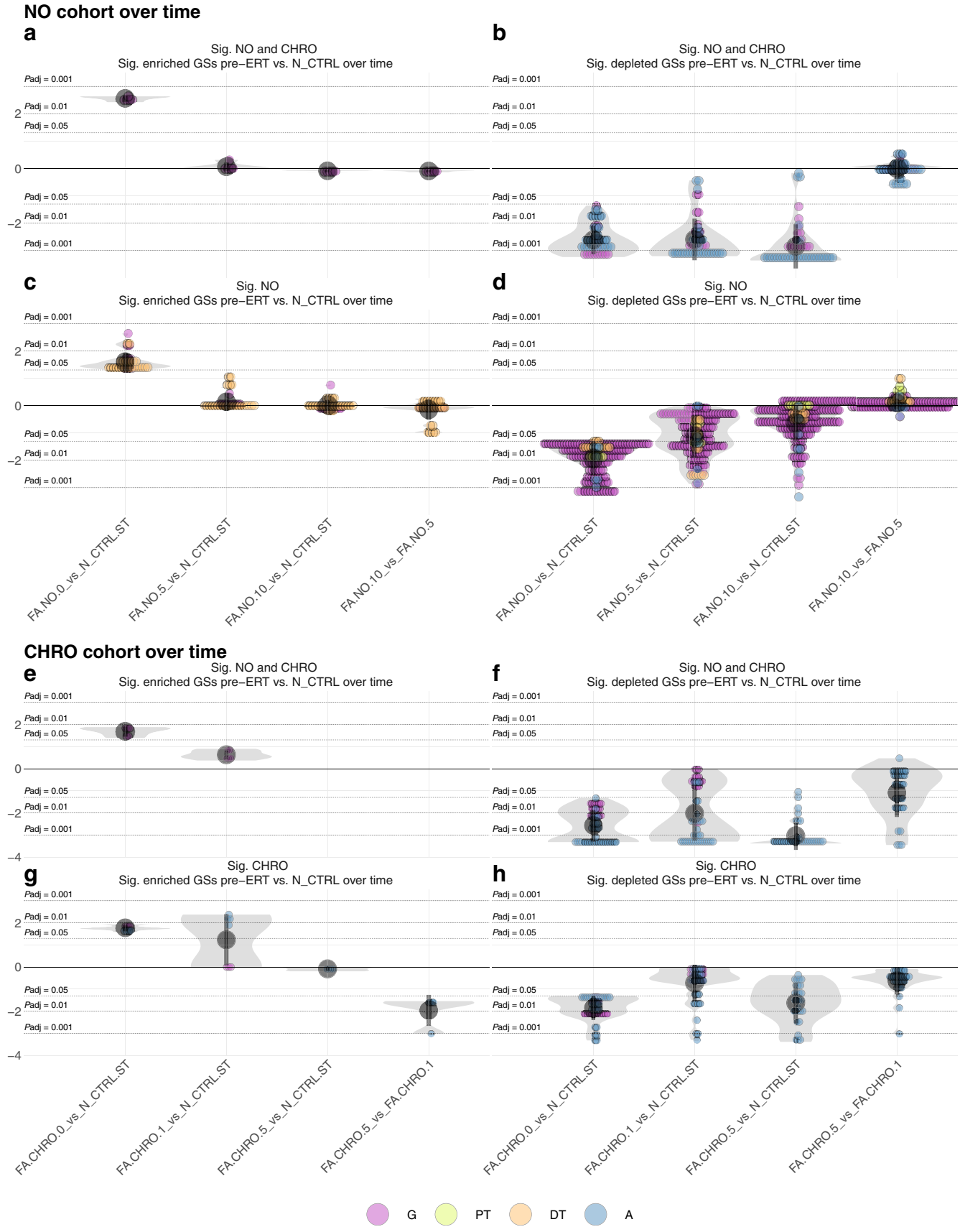

Figure 3 | Follow-up on gene sets (GSs) comprised in the comparative transcriptional landscapes over time. Violin plots displaying directional adjusted *P* values for any GS comprised in the transcriptional landscapes (Figures 1 and 2; Supplementary Figures S1 and S2). For this, adjusted *P* values were log transformed (log_{10}), and the algebraic sign was assigned according to enrichment (positive) (continued)

(Figure 5f) even after 10 years of ERT further underlines their relevance.

Systematic interpretation of the cross-validated glomerular transcriptional landscape pre-ERT and its modulation over time

The transcriptional landscape for glomeruli comprising cross-validated GSs identified enrichment pertaining to *Keratinization* and depletion in *Transporter and ion channel activity* (Figure 4a and b). In addition, 3 GSs with limited connectivity were also depleted (BIOLOGICAL OXIDATIONS, COLLAGEN-CONTAINING EXTRACELLULAR MATRIX, and DETECTION OF CHEMICAL STIMULUS), as shown in Figure 4a and b.

Assessing temporal evolvement during ERT revealed a clear dichotomy. *Keratinization* normalized to levels comparable with N_CTRLs after 1 year of ERT (Figure 4c) and remained stable for the entire follow-up period (Figure 4d and e). BIOLOGICAL OXIDATIONS and DETECTION OF CHEMICAL STIMULUS, on the other hand, appeared unaffected by ERT (Figure 4c–e), and original depletion of *Transporter and ion channel activity* was reversed over time (Figure 4c–e). Thus, analyzing genes underlying significant enrichment and depletion signals for these GSs (i.e., leading edge genes) calls for further investigation into these distinct response patterns.

As previously mentioned, enrichment of keratinization-associated processes was swiftly mitigated by ERT. Leading edge gene analysis resulted in a total of 8 genes that comparatively contributed to their significance in both patient groups (Figure 4f). However, no drug with known pharmacologic effects on the related protein products was registered in DrugBank 5.1.5's 13,511 drug entries.[32] Although statistically *TCHH* and *KRT6C* represent key targets, a broader functional understanding of keratins in podocytes is emerging.[33]

ERT-resistant genetic module in glomeruli

The persistence or gradual reemergence of all but keratinization-related GSs after up to 10 years of ERT when compared with N_CTRLs warrants identification of genes that govern this phenomenon. Indeed, they may represent a disease-related genetic module insufficiently targeted by ERT.

Of the 321 leading edge genes underlying GSs depleted in both patient groups pre-ERT versus N_CTRLs, 79 genes were significantly downregulated pre-ERT and failed to normalize to expression levels comparable to N_CTRLs in both cohorts at any time point during the 10-year follow-up ($P < 0.05$; Supplementary Figure S9A–E). Improving confidence, 32 of these genes were retained even when setting all thresholds to $P < 0.01$ (Figure 4g). Depending on these threshold levels, possible lysosomal localization was identified for 6 and 9 of the candidates, respectively (diamond-shaped symbols in Figure 4g and Supplementary Figure S9A–E).

Systematic interpretation of the cross-validated arterial transcriptional landscape pre-ERT and its modulation over time

The cross-validated arterial transcriptional landscape displays 3 clusters (Figure 5a and b). Interestingly, it shows alterations in biological themes similar to those identified for glomeruli (Figure 4a and b).

In contrast with glomeruli, *Keratinization* was depleted in arteries and ERT failed to modulate this cluster over time (Figure 5c–f). It also includes an additional 5 GSs that pertain to intermediate filament components in particular. For DETECTION OF CHEMICAL STIMULUS, although in glomeruli it was mapped as a single GS with limited connectivity (Figure 4a–e), in arteries it formed the center of the theme *Detect and respond to stimulus* (Figure 5a–f). The latter was composed of pathways not only related to detection but also response to stimuli (Figure 5a–f). For the third clusters, although thematically related, there was no overlap between the specific transport-related GSs cross-validated in either glomeruli or arteries (Figures 4a–e and 5a–f).

ERT-resistant genetic module in arteries

All cross-validated aspects defining arteries of FN, except 2 to 3 intermediate filament-associated GSs, remained depleted versus N_CTRLs irrespective of cohort, ERT, and follow-up

Figure 3 | (continued) or depletion (negative). Data from the patient cohort from Bergen, Norway (NO), are displayed in the upper half (**a–d**), and data from the validation cohort from Switzerland and Romania (CHRO) are displayed in the lower half (**e–h**). For adequate representation, GSs were also split according to if they were enriched (panels on the left; **a,c,e,g**) or depleted (panels on the right; **b,d,f,h**) in patients with Fabry disease (FD) before enzyme replacement therapy (ERT) versus N_CTRLs. To distinguish temporal development of GSs significantly (Sig.) changed in both cohorts pre-ERT versus N_CTRLs (**a,b,e,f**) or uniquely in 1 cohort versus N_CTRLs (**c,d,g,h**), the data were split further. For all panels, the solid horizontal line corresponds to an adjusted *P* of 1, whereas the dashed horizontal lines indicate significance levels of 0.05, 0.01, and 0.001 for enrichment and depletion, respectively. Bars indicate mean ± SD. A, arteries; DT, distal tubuli; G, glomeruli; FA.CHRO.0_vs_N_CTRL.ST, pre-ERT or ERT < 6 months from patients with FD belonging to the CHRO cohort versus normal controls; FA.CHRO.1_vs_N_CTRL.ST, 1-year post-initiation of ERT from patients with FD belonging to the CHRO cohort versus normal controls; FA.CHRO.5_vs_N_CTRL.ST, 5-years post-initiation of ERT from patients with FD belonging to the CHRO cohort versus normal controls; FA.CHRO.5_vs_FA.CHRO.1, 5-years post-initiation of ERT from patients with FD belonging to the CHRO cohort versus 1-year post-initiation of ERT from patients with FD belonging to the CHRO cohort; FA.NO.0_vs_N_CTRL.ST, pre-ERT from patients with FD belonging to the NO cohort versus normal controls; FA.NO.5_vs_N_CTRL.ST, 5-years post-initiation of ERT from patients with FD belonging to the NO cohort versus normal controls; FA.NO.10_vs_N_CTRL.ST, 10-years post-initiation of ERT from patients with FD belonging to the NO cohort versus normal controls; FA.NO.10_vs_FA.NO.5, 10-years post-initiation of ERT from patients with FD belonging to the NO cohort versus 5-years post-initiation of ERT from patients with FD belonging to the NO cohort.

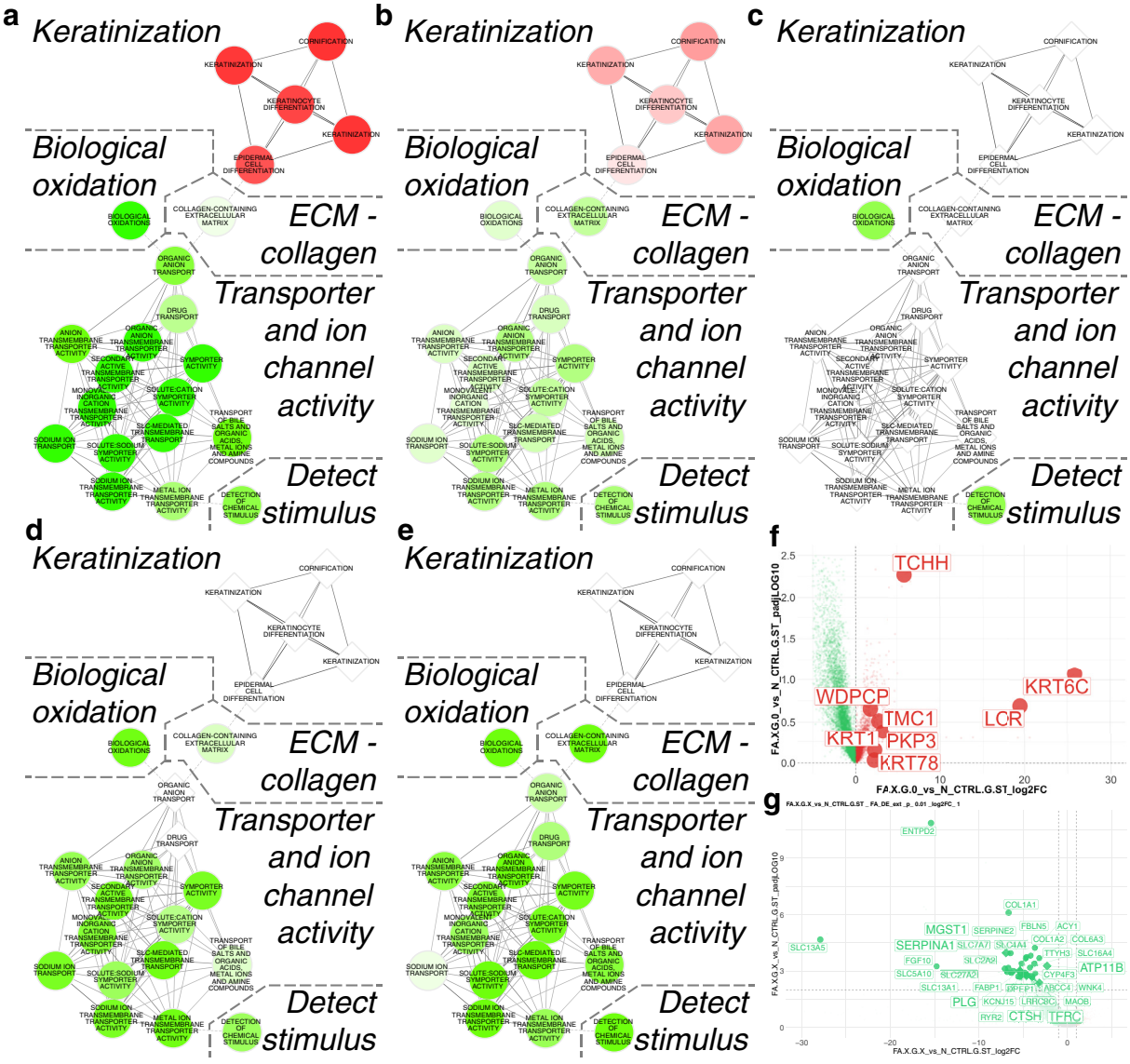

Figure 4| Cross cohort validated glomerular transcriptional landscape of Fabry disease (FD) before enzyme replacement therapy (ERT), its modulation in presence of ERT over 1, 5, and 10 years, and identification of an ERT-resistant genetic module. (**a–e**) Fast Gene Set Enrichment Analysis adjusted *P* values for (**a**) FA pre-ERT (patient cohort from Bergen, Norway [NO]) versus N_CTRLs, (**b**) FA pre-ERT (validation cohort from Switzerland and Romania [CHRO]) versus N_CTRLs, (**c**) FA 1 year after initiation of ERT (CHRO cohort) versus N_CTRLs, (**d**) FA 5 years after initiation of ERT (NO cohort) versus N_CTRLs, and (**e**) FA 10 years after initiation of ERT (NO cohort) versus N_CTRLs. (**a–e**) Node color: red hue correlates with significant enrichment; and green color hue correlates with significant depletion for the respective comparison. Node shape: ellipse = adjusted $P < 0.05$; and diamond = adjusted $P \geq 0.05$. Edge color: blackness correlates with the degree of member genes overlapping between the gene set (GS) members it connects. Edge line style: solid = connectivity ≥10% (regular edge); and dashed = connectivity <10% (extra edge ensuring a fully connected network). The prominent long-dashed lines segregate the network with respect to the major biological themes identified. (**f**) Volcano plot of all genes with valid individual adjusted *P* values consistently underlying the significant enrichment signals (leading edge [LE] genes) of the keratinization-related GSs in both FD cohorts versus N_CTRLs. The *x*-axis maps mean $\log_2$ fold changes, and the *y*-axis shows mean $\log_{10}$ transformed adjusted *P* values for NO cohort versus N_CTRLs and the CHRO cohort versus N_CTRLs. (**g**) Volcano plot displaying all genes underlying significant depletion signals in both FD cohorts versus N_CTRLs (LE genes) that were significantly downregulated (adjusted $P < 0.01$, fold change <−2) in every cohort and at every time point compared with N_CTRLs. The *x*-axis maps the corresponding average $\log_2$ fold changes, and the *y*-axis shows the corresponding average $\log_{10}$ transformed adjusted *P* values. Larger diamond-shaped symbols highlight genes whose protein products have reasonable probability for lysosome localization. ECM, extracellular matrix.

time (Figure 5c–f). As for glomeruli, exhibiting such resistance to modulation via ERT is a reason to assume that related downregulated genes, yielding significance across all comparisons versus N_CTRLs, may represent a relevant ERT-resistant genetic module. Volcano plots displaying these genes (adjusted $P < 0.05$) for *Keratinization and intermediate*

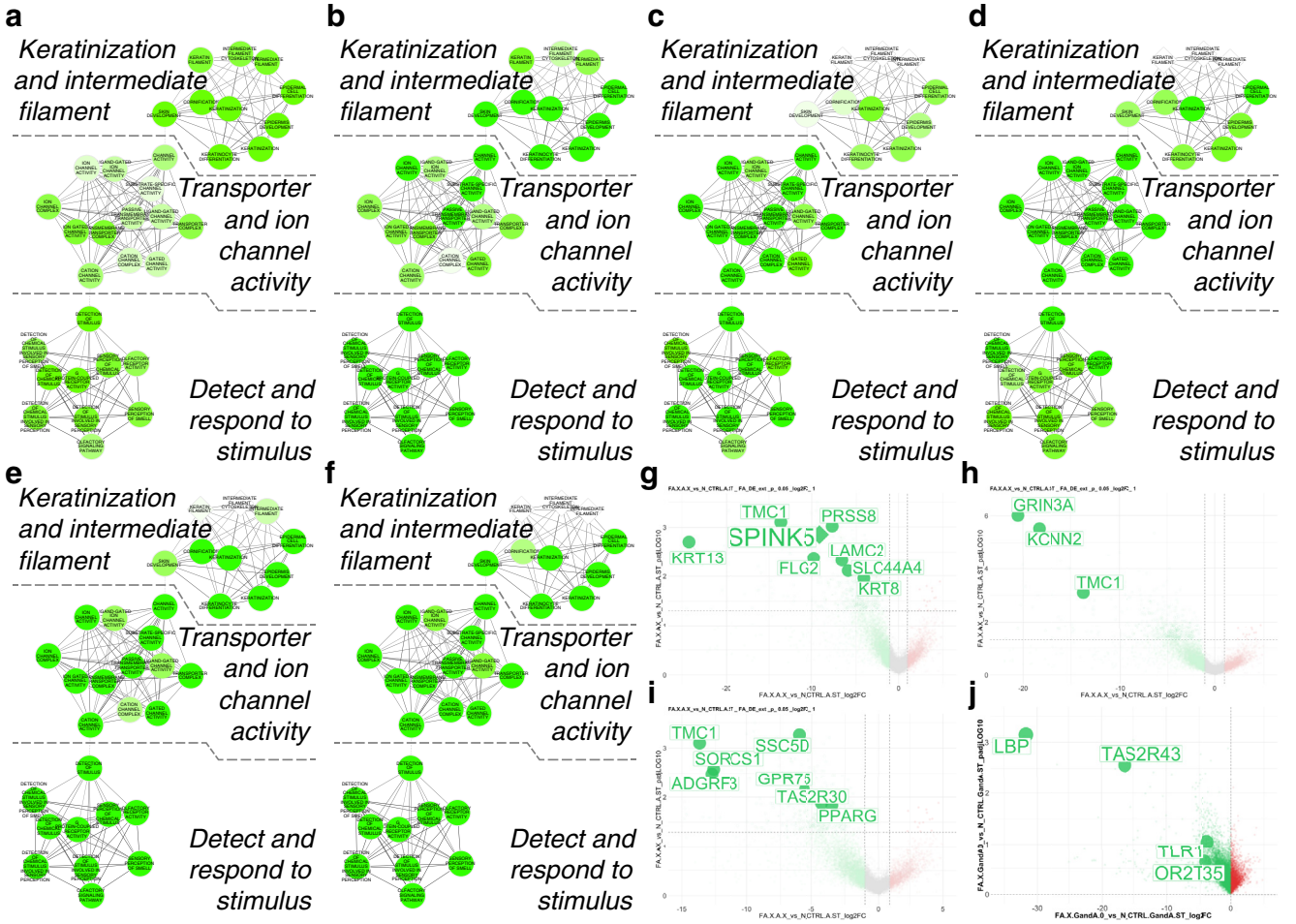

Figure 5 | Cross cohort validated arterial transcriptional landscape of Fabry nephropathy (FN) before enzyme replacement therapy (ERT) and its modulation in presence of ERT over 1, 5, and 10 years and identification of an ERT-resistant genetic module. (**a–f**) Fast Gene Set Enrichment Analysis adjusted *P* values for (**a**) FN pre-ERT (patient cohort from Bergen, Norway [NO]) versus N_CTRLs, (**b**) FN pre-ERT (validation cohort from Switzerland and Romania [CHRO]) versus N_CTRLs, (**c**) FN 1 year after initiation of ERT (CHRO cohort) versus N_CTRLs, (**d**) FN 5 years after initiation of ERT (NO cohort) versus N_CTRLs, (**e**) FN 5 years after initiation of ERT (CHRO cohort) versus N_CTRLs, and (**e**) FN 10 years post-initiation of ERT (NO-cohort) vs. N_CTRLs. (**a–f**) Node color: red hue correlates with significant enrichment; and green hue correlates with significant depletion for the respective comparison. Node shape: ellipse = adjusted $P < 0.05$; and diamond = adjusted $P \geq 0.05$. Edge color: blackness correlates with the degree of member genes overlapping between the gene set (GS) members it connects. Edge line style: solid = connectivity ≥10% (regular edge); and dashed = connectivity <10% (extra edge ensuring a fully connected network). The prominent long-dashed lines segregate the network with respect to the major biological themes identified. (**g**) Volcano plot displaying all genes underlying significant depletion signals for the *Keratinization and intermediate filament* cluster in both Fabry disease (FD) cohorts versus N_CTRLs (leading edge [LE] genes) that were significantly downregulated (adjusted $P < 0.05$, fold change <−2) in every cohort and at every time point compared with N_CTRLs. The *x*-axis maps the corresponding average $\log_2$ foldchanges, and the *y*-axis shows the corresponding average $\log_{10}$ transformed adjusted *P* values. Larger diamond-shaped symbols highlight genes whose protein products have reasonable probability for lysosome localization. (**h**) As (**g**) but displaying the respective genes identified within the *Transporter and ion channel activity* cluster. (**i**) As (**g**) but displaying the respective genes identified within the *Detect and respond to stimulus* cluster. (**j**) Volcano plot of all genes with valid individual adjusted *P* values consistently underlying the significant depletion signal (LE genes) of the *Detect stimulus* cluster in glomeruli and the *Detect and respond to stimulus* cluster in arteries of both FD cohorts versus N_CTRLs.

filament (Figure 5g), *Transporter and ion channel activity* (Figure 5h), and *Detect and respond to stimulus* (Figure 5i) identified a handful of candidates that exhibited such resistance to ERT. For all these candidates (Figure 5g–i), only *SPINK5*'s protein product was deemed to have potential lysosome localization. *TMC1*'s pleiotropy resulted in this gene contributing to GSs' significant depletion signal in all 3 clusters (Figure 5g–i).

Interrogating ERT-resistant genetic modules for known drug targets

A total of 94 genes consistently resisted modulation during ERT: 78 identified in glomeruli (Supplementary Figure S9A), 15 identified in arteries (Figure 5g–i), and *SLC44A4* identified in both compartments. After curating drug interactions for adequate pharmacologic action and drugs for developmental stage (approved, investigational, or experimental) using

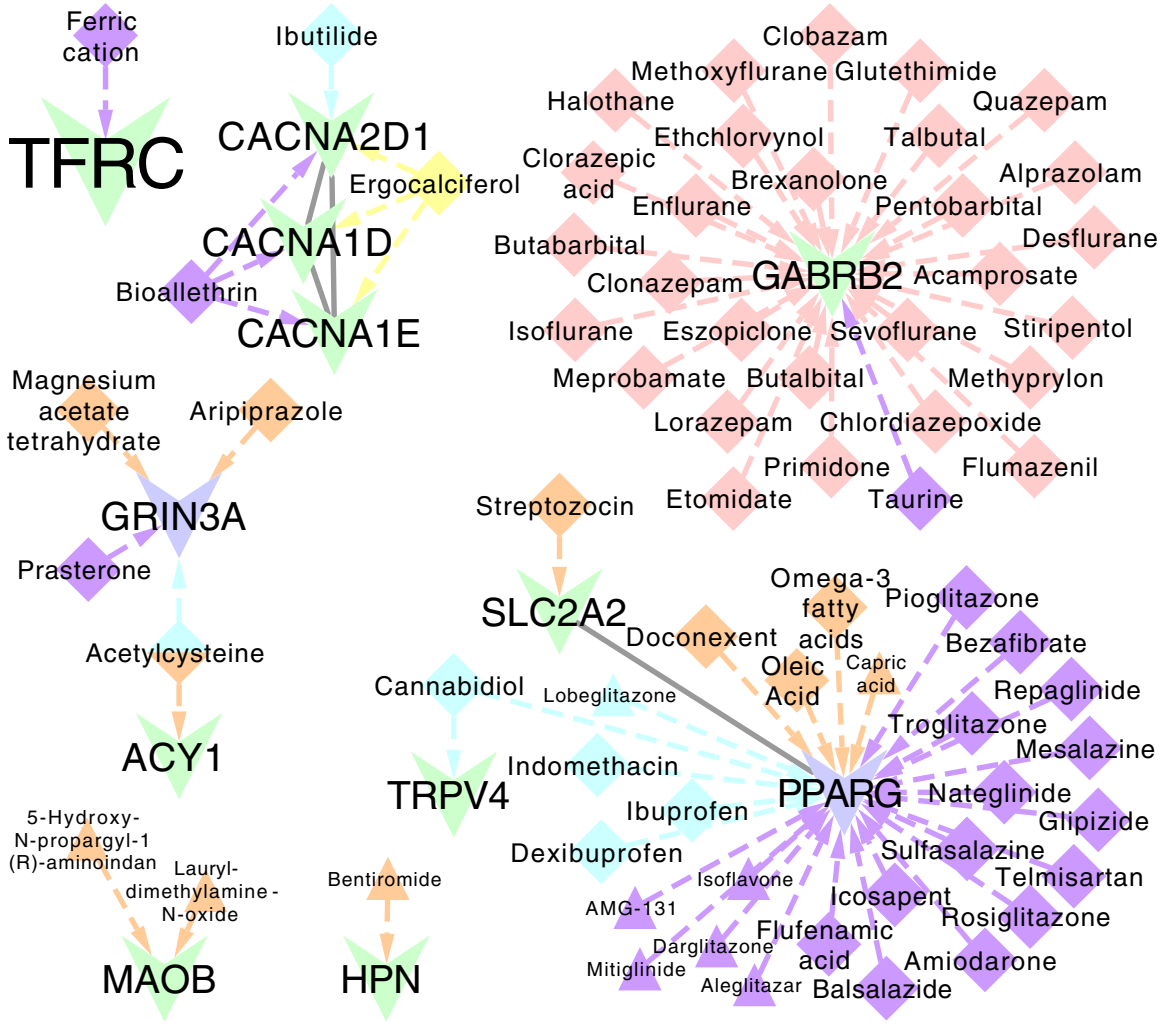

Figure 6 | Target::target::drug interactome for members of the enzyme replacement therapy–resistant genetic modules suitable for drug repurposing approaches. Target::target interactions were extracted from String V11 and subsequently integrated with drug::target interactions and pharmacologic action data listed in DrugBank 5.1.5. Displayed are 12 targets that can theoretically interact with the 69 drug candidates mapped. Node shape: large Y shape = target with predicted lysosomal localization, Y shape = target, diamond = approved drug, and triangle = experimental/investigational drug. Node color target: green = target defined in glomeruli, and blue = target defined in arteries. Edge target::target interaction = gray. Node and edge color target::drug interaction: activators = cyan, agonists = purple, inducers = yellow, ligands = orange, and positive modulators = red. ACY1, aminoacylase 1; GABRB2, gamma-aminobutyric acid type A receptor subunit beta2; GRIN3A, glutamate ionotropic receptor NMDA type subunit 3A; HPN, hepsin; MAOB, monoamine oxidase B; SLC2A2, solute carrier family 2 member 2; TFRC, transferrin receptor; TRPV4, transient receptor potential cation channel subfamily V member 4.

DrugBank 5.1.5,[32] 12 targets were mapped as potential targets that can theoretically interact with 69 possible drug candidates (Figure 6). Notably, 3 are interacting calcium voltage-gated channel-encoding genes, and *TFRC* was classified as having potential lysosome localization[30] (Figure 6). Disturbances in cellular and systemic iron levels are recognized as causes and consequences of kidney injury, and exploiting these mechanisms therapeutically has been proposed recently.[34]

Fidelity between RNAseq per kidney compartment and significant alterations in urine proteomics

Depending on factors, such as translational efficiency and physical properties, alterations in gene expression may translate to quantities of their protein products being detectable in biofluids. A study by Kurschat *et al.*, focusing on urine-derived primary cells of patients with FD, includes a proteomics data set,[35] allowing for such approximation via correlation analyses (Figure 7). Although no general correlation between RNAseq and proteomics was apparent, some molecules yielded significance in both data sets. In conjunction with particularly low expression of α-galactosidase A, glomeruli and arteries again provided the most meaningful data points (Figure 7). Notably, *TFRC*, a member of the ERT-resistant and lysosome-associated module (Figure 4g) in glomeruli and its ligand transferrin (TF), significantly downregulated in arteries, could be confirmed in such a manner (Figure 7).

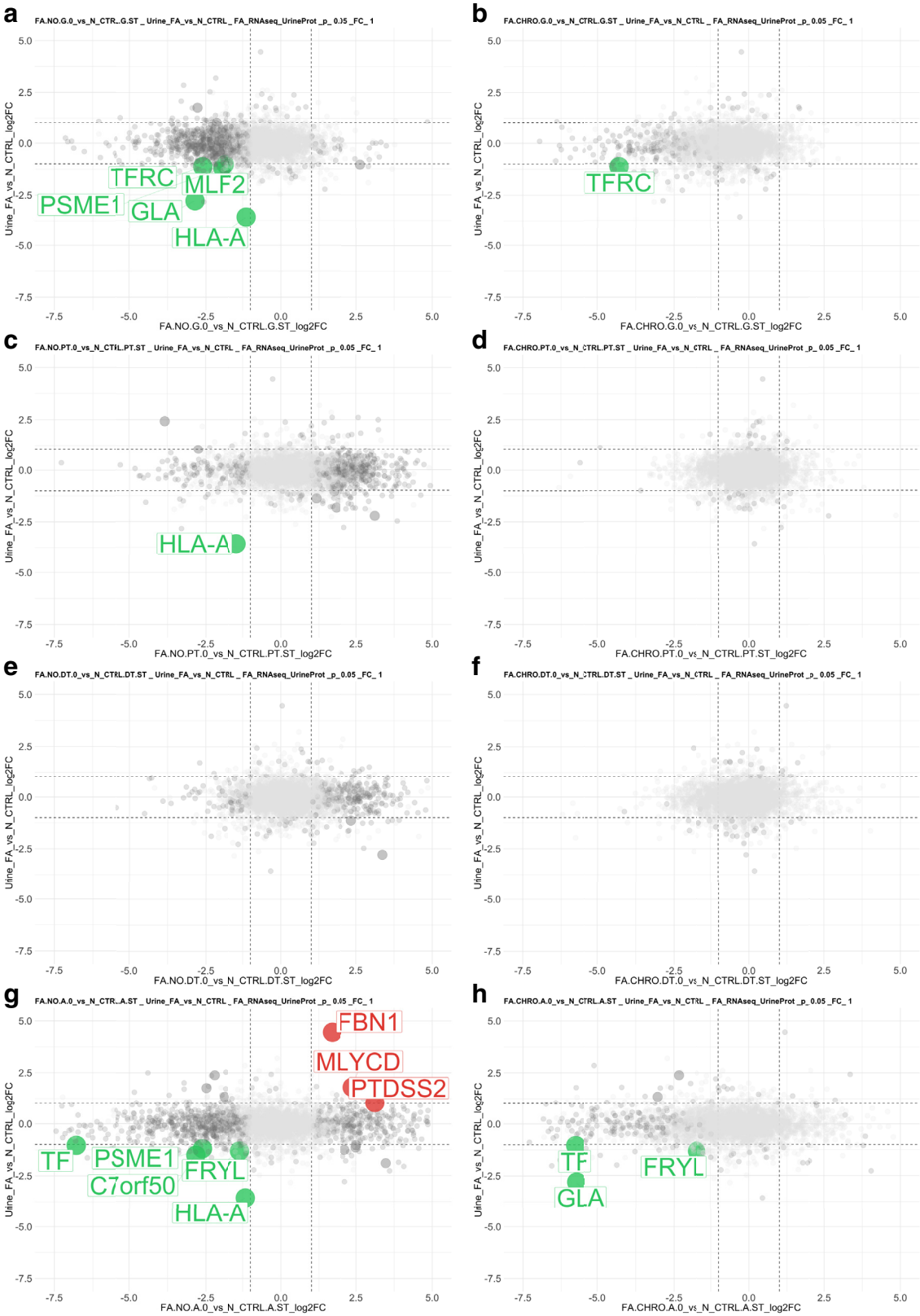

Figure 7 | Integrating RNA-sequencing (RNAseq) data per compartment and per cohort with urine-derived primary cell proteomics data. Scatterplots display the $\log_2$ fold-change proteomics data (Fabry disease [FD] vs. N_CTRLs) on the *x*-axis versus the respective RNAseq comparison mapped on the *y*-axis. Components that passed thresholds of adjusted $P < 0.05$ and fold change >2 (red) or <−2 (green) for gene expression and proteomics are highlighted and annotated. (**a**) Glomeruli before enzyme replacement therapy (ERT) (patient cohort from Bergen, Norway [NO]) versus N_CTRLs. (**b**) Glomeruli pre-ERT (validation cohort from Switzerland and Romania [CHRO]) versus (continued)

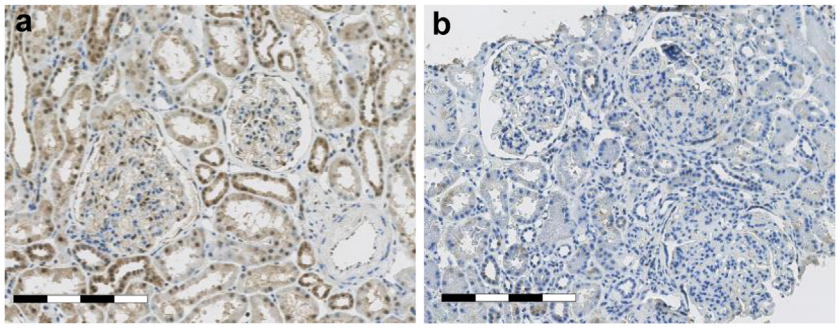

Figure 8 | Immunohistochemistry of transferrin receptor (TFRC). (**a**) Normal control tissue showing distinct glomerular positivity of TFRC. (**b**) A 10-year biopsy of a patient with Fabry nephropathy under enzyme replacement therapy demonstrates distinctively less TFRC staining in glomeruli. Bar = 100 μm. To optimize viewing of this image, please see the online version of this article at www.kidney-international.org.

Validation of transferrin receptor protein localization via immunohistochemistry

Analyses from mRNA abundances revealed that *TFRC* had a lower expression in glomeruli with FN at all time points, compared with normal controls. Immunohistochemistry of the transferrin receptor (TFRC) in kidney biopsies confirmed lower glomerular synthesis of TFRC proteins in a patient treated with 10 years of ERT compared with a healthy control (Figure 8a and b).

DISCUSSION

This study contributes to the understanding of the complex mechanisms involved in FD by (i) delineating its molecular characteristics in 4 kidney compartments of 2 independent cohorts and (ii) proposing cross-validated molecular modules with druggable components that consistently resisted modulation via ERT over time. The methods for data acquisition and analysis presented here further represent an applicable concept of how to unlock understanding and tangible discoveries from unique archival biobank materials.[18,36] With respect to clinical relevance, such studies will likely surpass insights gained via *in vivo* or *in vitro* models alone.[37–39]

Delineation and integration of transcriptional landscapes from 2 small, but independent, FD cohorts allowed delineation of the molecular basis underlying some of the commonly observed intercohort heterogeneity. Although the absence of any pathway diametrically opposing the 2 cohorts inspires confidence, it nevertheless puts high demands on choosing an adequate strategy to gain insights. In this study, limiting false positives was strictly prioritized. This does not mean that other data points made available via this study's deposited raw data and findings presented in a structured manner in the Supplementary Materials will not facilitate future hypothesis-driven studies. In situations without direct experimental verification, cross-validation is important, especially if these aspects simultaneously point to mechanisms unaffected by ERT. In any case, these results should encourage collaboration to expand cohort size and emphasize the need for academia-industry collaborations in the area of drug development.[40]

Currently, several new strategies for treatment of FD are being investigated. As prominent examples, substrate reduction therapy,[41] chaperone therapy,[42,43] plant-based production,[44] pegunigalsidase-α (PEGylated enzyme),[45] encapsulated mRNA,[46] and gene therapy[47,48] have either been licensed or are being evaluated in clinical studies.

Considering this situation, one might question the place of systems-focused analyses such as presented here. Regarding the requirement of an amenable mutation for successful chaperone treatment,[42,43] this treatment is still limited to 37% to 60% of patients based on whether there is an amenable variant.[49–51] This makes it paramount to deepen our understanding beyond the visible histologic alterations in the kidney.

The data presented here may be leveraged to help answer several long-standing questions in FD. There is, for example, an ongoing discussion about when to start ERT, especially in asymptomatic or oligosymptomatic patients. The high costs of ERT and the need for infusions every other week, together with possible adverse effects, may make starting ERT too early seem undesirable. Starting ERT too late, however, also poses risks to the patient's health.[52,53] Our results pointing to the relevance of age when initiating ERT also suggest candidates that, based on changes in mRNA expression, precede clinical alterations and may guide decisions, leading to a more informed time point to start ERT. Such repeatedly measurable biomarkers may especially be valuable in conjunction with already established markers, such as lysosomal GL-3.[54]

One adverse effect of ERT is the formation of anti-drug antibodies[48,52,53] in some individuals. Although no such patient was included here, there is a possibility to investigate this

Figure 7 | (continued) N_CTRLs. (**c**) Proximal tubuli pre-ERT (NO cohort) versus N_CTRLs. (**d**) Proximal tubuli pre-ERT (CHRO cohort) versus N_CTRLs. (**e**) Distal tubuli pre-ERT (NO cohort) versus N_CTRLs. (**f**) Distal tubuli pre-ERT (CHRO cohort) versus N_CTRLs. (**g**) Arteries pre-ERT (NO cohort) versus N_CTRLs. (**h**) Arteries pre-ERT (CHRO cohort) versus N_CTRLs.

phenomenon and its possible mitigation via immunomodulation by integrating this data set with corresponding data from patients with FN presenting these antibodies.

Well in accordance with their transcriptome, the NO cohort showed no significant differences in clinical parameters when comparing baseline with 10-years postinitiation of ERT. Likely a result of timely initiation of ERT, we nevertheless measured changes in plasma GL-3 levels known to correlate with reduced or absent α-galactosidase activity. Detectable in advance of clinical symptoms,[55] this presents a strong argument to continue acquiring omics data during follow-up. Not only would we gain additional molecular data underlying clinical presentation of FN, but we could also estimate the predictive value of molecular alterations present at earlier time points.

From the point of inferring clinical applications, one might also use this data set as a reference to estimate the degree of fidelity between the kidney's system state and biomarkers measured in urine. Understanding relations of biomarkers when measured in target tissues and when detected in easily and repetitively collectable biofluids, it may significantly reduce dependency on biopsies, as we have suggested, for other diseases.[56,57] This also opens new avenues for better patient management via tracking disease course and treatment responses via biomarker-based criteria. Integrating FFPE RNAseq data with urine proteomics delivered first encouraging results in this study. Although not investigated in this article, urinary exosomes are an interesting and emerging field of study in this regard.[58]

LCM of the kidney's major compartments also allowed gaining important spatial information. Clearly, glomeruli as the most heterogeneous compartment also displayed the most extensive molecular alterations. The transcriptional changes in arteries were the most consistent across cohorts. This correlates well with the morphometric changes in arteries in FD and is of clinical relevance.[59] Also, as a result of LCM, activation of different classes of immune processes in distal tubuli and arteries was detectable. Nevertheless, once computational molecular signature-based expression deconvolution allows approximation of cellular composition from bulk kidney,[40] LCM may lose some of its advantages and give way to greater sequencing depth of coverage or lowering requirements on mRNA quantity. Also, once spatial transcriptomics is established, understanding of the different nephron compartments could be increased on basis of this technology.[60]

With ERT as a well-established primary treatment option, we present molecular data that underpin its effectiveness in mitigating FN in different kidney compartments. This effect was particularly substantial and long lasting in the NO cohort. More important, these patients received ERT early[16] and essentially retained significant organ function over time (Table 1). Although the data available for the CHRO cohort precluded assessing these points in similar detail, the situation after short periods of ERT still suggests favorable effects of timely ERT.[16,61]

Despite of ERT's substantial impact on transcriptional landscapes of FN, it seemed least effective readjusting gene-expression patterns in arteries to levels comparable to N_CTRLs irrespective of cohort. With cardiovascular disease and cerebrovascular events as primary causes of shortened life expectancy in patients with FD, persistence of vascular abnormalities on a molecular level despite ERT is relevant and supports previous morphometric findings.[59]

Nonetheless, this work also has several limitations. Although we did not observe any obvious differences between different types of ERT, we were unable to assess such effects formally. Another limitation concerns the relatively small number of patients from whom such well-documented, complete, and temporal RNAseq profiles could be generated. Related to this issue, only 1 somewhat skewed control group could be included. This is especially true for the CHRO cohort and also affects the comparability of the cohorts *per se*, including aspects such as age, sex (inferred from biological attributes), environment, and baseline measurements (Table 1). These concerns are relevant and have critically shaped our data analysis strategy. Through minimizing to a significant degree introduction of type 1 errors, there is reason to believe that these findings are thus relevant for a broad range of patients with FD.

In conclusion, although personalized medicine should not, for the time being, be considered as a pragmatic strategy for developing novel treatments, insight gained via "omics" technologies may nonetheless guide development of precision medicine for FD. This is especially valid if candidates are classified as targets of existing drugs that may be repurposed as a treatment adjunct to ERT. The druggable aspects of the ERT-resistant module in general and the TFRC::TF axis in particular seem to lend themselves to exploring such strategies.

DISCLOSURE

ES reports receiving a grant from Sanofi Genzyme; positions on the advisory boards of Amicus and Sanofi-Genzyme; and speaker fees and travel support from Amicus, Sanofi-Genzyme, and Shire-Takeda, all outside of the submitted work. CT has obtained speaker fees and travel support from Amicus, Sanofi-Genzyme, and Shire-Takeda. H-PM reports receiving grants from Alexion, Amicus, Sanofi-Genzyme, and Shire-Takeda. AN received research support, travel support, and speaker honoraria from Sanofi Genzyme, Takeda, and Amicus. OE received travel support from Sanofi-Genzyme and Takeda. SL received travel support and speaker fees from Sanofi-Genzyme.

DATA STATEMENT

The data supporting the findings of this study are openly available in the repository Gene Expression Omnibus (GEO) at https://www.ncbi.nlm.nih.gov/geo/ with accession number GSE178947.

ACKNOWLEDGMENTS

We thank the staff from the Functional Genomics Center Zurich (FGCZ), ETH Zurich and University of Zurich, Zurich, Switzerland, Firalis S.A., Huningue, France, Genomics Core Facility (GCF), and Norwegian University of Science and Technology (NTNU) for RNA library preparation, sequencing, and data processing. GCF is funded

by the Faculty of Medicine at the Norwegian University of Science and Technology (NTNU), Trondheim, Norway, and the Central Norway Regional Health Authority, Stjørdal, Norway. We also acknowledge Gener Ismail for performing the kidney biopsies at the Fundeni Clinical Institute, Bucharest, Romania. This work is supported by an open project grant from the Western Norway Regional Health Authority to H-PM (Helse Vest grant 912233) and by research grants from Sanofi-Genzyme, Shire-Takeda, and Amicus Therapeutics to H-PM.

AUTHOR CONTRIBUTIONS

H-PM, OE, and ND designed the study; OE, TO, MS, and PS performed experiments. ND, AF, H-PM, and OE processed and/or analyzed the RNA-sequencing data (ND developed the data analyses strategies and respective methods). IK preprocessed and quality controlled the RNA-sequencing data. SL reviewed the nephropathological sections. ND made Figures 1–7 and Supplementary Figures S1–S9. TO and PS made Figure 8. ND, HPM, OE, and PS drafted the article. RS, CT, ES, AG, AN, and ER helped with patient selection, provided kidney biopsies, and obtained clinical patient data. All authors approved the final version of the article.

SUPPLEMENTARY MATERIAL

Supplementary File (PDF)

Supplementary Figure S1. Comparative gene set (GS)–based transcriptional landscape of glomeruli integrating similarities and differences between the patient cohort from Bergen, Norway (NO) and validation cohort from Switzerland and Romania (CHRO) before enzyme replacement therapy (ERT) versus N_CTRLs.

Supplementary Figure S2. Comparative gene set (GS)–based transcriptional landscape of arteries integrating similarities and differences between the patient cohort from Bergen, Norway (NO) and validation cohort from Switzerland and Romania (CHRO) before enzyme replacement therapy (ERT) versus N_CTRLs.

Supplementary Figure S3. Comparative gene set (GS)–based transcriptional landscape of proximal tubuli integrating similarities and differences between the patient cohort from Bergen, Norway (NO) and validation cohort from Switzerland and Romania (CHRO) before enzyme replacement therapy (ERT) versus N_CTRLs.

Supplementary Figure S4. Comparative gene set (GS)–based transcriptional landscape of distal tubuli integrating similarities and differences between the patient cohort from Bergen, Norway (NO) and validation cohort from Switzerland and Romania (CHRO) before enzyme replacement therapy (ERT) versus N_CTRLs.

Supplementary Figure S5. Evolvement of the comparative gene set (GS)–based transcriptional landscape of glomeruli from before enzyme replacement therapy (ERT) to 10 years after initiation of ERT.

Supplementary Figure S6. Evolvement of the comparative gene set (GS)–based transcriptional landscape of proximal tubuli from before enzyme replacement therapy (ERT) to 10 years after initiation of ERT.

Supplementary Figure S7. Evolvement of the comparative gene set (GS)–based transcriptional landscape of distal tubuli from before enzyme replacement therapy (ERT) to 10 years after initiation of ERT.

Supplementary Figure S8. Evolvement of the comparative gene set (GS)–based transcriptional landscape of arteries from before enzyme replacement therapy (ERT) to 10 years after initiation of ERT.

Supplementary Figure S9. Volcano plots of the entire enzyme replacement therapy (ERT)–resistant genetic module identified in glomeruli and per biological theme.

Supplementary Glossary. Glossary of concept for studying complex systems in context with precision medicine relevant to this study.

REFERENCES

1. Eikrem O, Skrunes R, Tondel C, et al. Pathomechanisms of renal Fabry disease. *Cell Tissue Res*. 2017;369:53–62.
2. Hopkin RJ, Bissler J, Banikazemi M, et al. Characterization of Fabry disease in 352 pediatric patients in the Fabry registry. *Pediatr Res*. 2008;64:550–555.
3. Wilcox WR, Oliveira JP, Hopkin RJ, et al. Females with Fabry disease frequently have major organ involvement: lessons from the Fabry registry. *Mol Genet Metab*. 2008;93:112–128.
4. Fogo AB, Bostad L, Svarstad E, et al. Scoring system for renal pathology in Fabry disease: report of the International Study Group of Fabry Nephropathy (ISGFN). *Nephrol Dial Transplant*. 2010;25:2168–2177.
5. Branton M, Schiffmann R, Kopp JB. Natural history and treatment of renal involvement in Fabry disease. *J Am Soc Nephrol*. 2002;13(suppl 2): S139–S143.
6. Tondel C, Bostad L, Hirth A, et al. Renal biopsy findings in children and adolescents with Fabry disease and minimal albuminuria. *Am J Kidney Dis*. 2008;51:767–776.
7. Germain DP. Fabry disease. *Orphanet J Rare Dis*. 2010;5:30.
8. Spada M, Baron R, Elliott PM, et al. The effect of enzyme replacement therapy on clinical outcomes in paediatric patients with Fabry disease - a systematic literature review by a European panel of experts. *Mol Genet Metab*. 2019;126:212–223.
9. Rombach SM, Smid BE, Bouwman MG, et al. Long term enzyme replacement therapy for Fabry disease: effectiveness on kidney, heart and brain. *Orphanet J Rare Dis*. 2013;8:47.
10. Meikle PJ, Hopwood JJ, Clague AE, et al. Prevalence of lysosomal storage disorders. *JAMA*. 1999;281:249–254.
11. Beckmann JS, Lew D. Reconciling evidence-based medicine and precision medicine in the era of big data: challenges and opportunities. *Genome Med*. 2016;8:134.
12. Scannell JW, Blanckley A, Boldon H, et al. Diagnosing the decline in pharmaceutical R&D efficiency. *Nat Rev Drug Discov*. 2012;11:191–200.
13. Schee Genannt Halfmann S, Mahlmann L, Leyens L, et al. Personalized medicine: what's in it for rare diseases? *Adv Exp Med Biol*. 2017;1031: 387–404.
14. Agache I, Akdis CA. Precision medicine and phenotypes, endotypes, genotypes, regiotypes, and theratypes of allergic diseases. *J Clin Invest*. 2019;130:1493–1503.
15. Delavan B, Roberts R, Huang R, et al. Computational drug repositioning for rare diseases in the era of precision medicine. *Drug Discov Today*. 2018;23:382–394.
16. Tondel C, Bostad L, Larsen KK, et al. Agalsidase benefits renal histology in young patients with Fabry disease. *J Am Soc Nephrol*. 2013;24:137–148.
17. Smid BE, Rombach SM, Aerts JM, et al. Consequences of a global enzyme shortage of agalsidase beta in adult Dutch Fabry patients. *Orphanet J Rare Dis*. 2011;6:69.
18. Eikrem O, Beisland C, Hjelle K, et al. Transcriptome sequencing (RNAseq) enables utilization of formalin-fixed, paraffin-embedded biopsies with clear cell renal cell carcinoma for exploration of disease biology and biomarker development. *PLoS One*. 2016;11:e0149743.
19. Johnson WE, Li C, Rabinovic A. Adjusting batch effects in microarray expression data using empirical Bayes methods. *Biostatistics*. 2007;8: 118–127.
20. Love MI, Huber W, Anders S. Moderated estimation of fold change and dispersion for RNA-seq data with DESeq2. *Genome Biol*. 2014;15:550.
21. Sergushichev AA. An algorithm for fast preranked gene set enrichment analysis using cumulative statistic calculation. Preprint. bioRxiv. 060012. Posted online June 20, 2016. https://doi.org/10.1101/060012
22. Subramanian A, Tamayo P, Mootha VK, et al. Gene set enrichment analysis: a knowledge-based approach for interpreting genome-wide expression profiles. *Proc Natl Acad Sci U S A*. 2005;102:15545–15550.
23. Merico D, Isserlin R, Stueker O, et al. Enrichment map: a network-based method for gene-set enrichment visualization and interpretation. *PLoS One*. 2010;5:e13984.
24. Eikrem O, Lillefosse B, Delaleu N, et al. Network-based assessment of minimal change disease identifies glomerular response to IL-7 and IL-12 pathways activation as innovative treatment target. *Biomedicines*. 2023;11:266.
25. Delaleu N, Nguyen CQ, Tekle KM, et al. Transcriptional landscapes of emerging autoimmunity: transient aberrations in the targeted tissue's extracellular milieu precede immune responses in Sjogren's syndrome. *Arthritis Res Ther*. 2013;15:R174.

26. Chen J, Guccini I, Di Mitri D, et al. Compartmentalized activities of the pyruvate dehydrogenase complex sustain lipogenesis in prostate cancer. *Nat Genet*. 2018;50:219–228.
27. Di Mitri D, Vasilevska J, Calcinotto A, et al. Re-education of tumor-associated macrophages by CXCR2 blockade drives senescence enhancement and tumor inhibition in advanced prostate cancer. *Cell Rep*. 2019;28:2156–2168.e5.
28. Emming S, Bianchi N, Polletti S, et al. A molecular network regulating the proinflammatory phenotype of human memory T lymphocytes. *Nat Immunol*. 2020;21:388–399.
29. Su G, Morris JH, Demchak B, et al. Biological network exploration with Cytoscape 3. *Curr Protoc Bioinformatics*. 2014;47:8.13.1–24.
30. Binder JX, Pletscher-Frankild S, Tsafou K, et al. COMPARTMENTS: unification and visualization of protein subcellular localization evidence. *Database (Oxford)*. 2014;2014:bau012.
31. Szklarczyk D, Gable AL, Lyon D, et al. STRING v11: protein-protein association networks with increased coverage, supporting functional discovery in genome-wide experimental datasets. *Nucleic Acids Res*. 2019;47:D607–D613.
32. Wishart DS, Feunang YD, Guo AC, et al. DrugBank 5.0: a major update to the DrugBank database for 2018. *Nucleic Acids Res*. 2018;46:D1074–D1082.
33. Schell C, Huber TB. The evolving complexity of the podocyte cytoskeleton. *J Am Soc Nephrol*. 2017;28:3166–3174.
34. van Swelm RPL, Wetzels JFM, Swinkels DW. The multifaceted role of iron in renal health and disease. *Nat Rev Nephrol*. 2020;16:77–98.
35. Slaats GG, Braun F, Hoehne M, et al. Urine-derived cells: a promising diagnostic tool in Fabry disease patients. *Sci Rep*. 2018;8:11042.
36. Marczyk M, Fu C, Lau R, et al. The impact of RNA extraction method on accurate RNA sequencing from formalin-fixed paraffin-embedded tissues. *BMC Cancer*. 2019;19:1189.
37. Leenaars CHC, Kouwenaar C, Stafleu FR, et al. Animal to human translation: a systematic scoping review of reported concordance rates. *J Transl Med*. 2019;17:223.
38. Rhrissorrakrai K, Belcastro V, Bilal E, et al. Understanding the limits of animal models as predictors of human biology: lessons learned from the sbv IMPROVER Species Translation Challenge. *Bioinformatics*. 2015;31:471–483.
39. Delaleu N, Nguyen CQ, Peck AB, et al. Sjogren's syndrome: studying the disease in mice. *Arthritis Res Ther*. 2011;13:217.
40. Berry SA, Coughlin CR 2nd, McCandless S, et al. Developing interactions with industry in rare diseases: lessons learned and continuing challenges. *Genet Med*. 2020;22:219–226.
41. Guerard N, Oder D, Nordbeck P, et al. Lucerastat, an iminosugar for substrate reduction therapy: tolerability, pharmacodynamics, and pharmacokinetics in patients with Fabry disease on enzyme replacement. *Clin Pharmacol Ther*. 2018;103:703–711.
42. Germain DP, Hughes DA, Nicholls K, et al. Treatment of Fabry's disease with the pharmacologic chaperone migalastat. *N Engl J Med*. 2016;375:545–555.
43. Hughes DA, Nicholls K, Shankar SP, et al. Oral pharmacological chaperone migalastat compared with enzyme replacement therapy in Fabry disease: 18-month results from the randomised phase III ATTRACT study. *J Med Genet*. 2017;54:288–296.
44. Kizhner T, Azulay Y, Hainrichson M, et al. Characterization of a chemically modified plant cell culture expressed human α-galactosidase-A enzyme for treatment of Fabry disease. *Mol Genet Metab*. 2015;114:259–267.
45. Schiffmann R, Goker-Alpan O, Holida M, et al. Pegunigalsidase alfa, a novel PEGylated enzyme replacement therapy for Fabry disease, provides sustained plasma concentrations and favorable pharmacodynamics: a 1-year phase 1/2 clinical trial. *J Inherit Metab Dis*. 2019;42:534–544.
46. DeRosa F, Smith L, Shen Y, et al. Improved efficacy in a Fabry disease model using a systemic mRNA liver depot system as compared to enzyme replacement therapy. *Mol Ther*. 2019;27:878–889.
47. Feriozzi S, Hughes DA. New drugs for the treatment of Anderson-Fabry disease. *J Nephrol*. 2021;34:221–230.
48. Felis A, Whitlow M, Kraus A, et al. Current and investigational therapeutics for Fabry disease. *Kidney Int Rep*. 2020;5:407–413.
49. Wu X, Katz E, Della Valle MC, et al. A pharmacogenetic approach to identify mutant forms of alpha-galactosidase A that respond to a pharmacological chaperone for Fabry disease. *Hum Mutat*. 2011;32:965–977.
50. Benjamin ER, Della Valle MC, Wu X, et al. The validation of pharmacogenetics for the identification of Fabry patients to be treated with migalastat. *Genet Med*. 2017;19:430–438.
51. Muntze J, Gensler D, Maniuc O, et al. Oral chaperone therapy migalastat for treating Fabry disease: enzymatic response and serum biomarker changes after 1 year. *Clin Pharmacol Ther*. 2019;105:1224–1233.
52. Cairns T, Muntze J, Gernert J, et al. Hot topics in Fabry disease. *Postgrad Med J*. 2018;94:709–713.
53. Schiffmann R, Hughes DA, Linthorst GE, et al. Screening, diagnosis, and management of patients with Fabry disease: conclusions from a "Kidney Disease: Improving Global Outcomes" (KDIGO) Controversies Conference. *Kidney Int*. 2017;91:284–293.
54. Nowak A, Mechtler TP, Hornemann T, et al. Genotype, phenotype and disease severity reflected by serum LysoGb3 levels in patients with Fabry disease. *Mol Genet Metab*. 2018;123:148–153.
55. Eng CM, Fletcher J, Wilcox WR, et al. Fabry disease: baseline medical characteristics of a cohort of 1765 males and females in the Fabry registry. *J Inherit Metab Dis*. 2007;30:184–192.
56. Delaleu N, Mydel P, Brun JG, et al. Sjogren's syndrome patients with ectopic germinal centers present with a distinct salivary proteome. *Rheumatology (Oxford)*. 2016;55:1127–1137.
57. Delaleu N, Mydel P, Kwee I, et al. High fidelity between saliva proteomics and the biologic state of salivary glands defines biomarker signatures for primary Sjogren's syndrome. *Arthritis Rheumatol*. 2015;67:1084–1095.
58. Street JM, Koritzinsky EH, Glispie DM, et al. Urine exosomes: an emerging trove of biomarkers. *Adv Clin Chem*. 2017;78:103–122.
59. Rombach SM, van den Bogaard B, de Groot E, et al. Vascular aspects of Fabry disease in relation to clinical manifestations and elevations in plasma globotriaosylsphingosine. *Hypertension*. 2012;60:998–1005.
60. Marx V. Method of the year: spatially resolved transcriptomics. *Nat Methods*. 2021;18:9–14.
61. Arends M, Wijburg FA, Wanner C, et al. Favourable effect of early versus late start of enzyme replacement therapy on plasma globotriaosylsphingosine levels in men with classical Fabry disease. *Mol Genet Metab*. 2017;121:157–161.